CZECH TECHNICAL
UNIVERSITY IN PRAGUE

FACULTY OF MECHANICAL
ENGINEERING

DEPARTMENT OF
MATERIALS ENGINEERING

NITI ALLOY PRODUCED BY COLD SPRAY

2023

TOMÁŠ HELLER

ZADÁNÍ BAKALÁŘSKÉ PRÁCE

I. OSOBNÍ A STUDIJNÍ ÚDAJE

Příjmení: **Heller** Jméno: **Tomáš** Osobní číslo: **501395**

Fakulta/ústav: **Fakulta strojní**

Zadávající katedra/ústav: **Ústav materiálového inženýrství**

Studijní program: **Teoretický základ strojního inženýrství**

Studijní obor: **bez oboru**

II. ÚDAJE K BAKALÁŘSKÉ PRÁCI

Název bakalářské práce:

Slitina NiTi připravená technologií studené kinetizace

Název bakalářské práce anglicky:

NiTi alloy produced by cold spray

Pokyny pro vypracování:

1. Vypracovat rešerši o základních charakteristikách technologie studené kinetizace.
2. Vypracovat rešerši o fenoménu tvarové paměti.
3. Provést charakterizaci vstupního prášku NiTi z pohledu morfologie, chemického a fázového složení.
4. Provést analýzu distribuce velikosti částic.

Seznam doporučené literatury:

1. Papyrin, Kosarev, Klinkov, Alkhimov, Fomin: Cold Spray Technology. Elsevier Science, 2006.
2. Schmidt, Assadi, Gartner, Richter, Stoltenhoff, Kreye, Klassen: From Particle Acceleration to Impact and Bonding in Cold Spraying. Journal of Thermal Spray Technology, 18, 2009, 794.
3. Jani, Leary, Subic, Gibson: A review of shape memory alloy research, applications and opportunities. Materials and Design, 56, 2014, 1078.
4. Mauer, Rauwald, Sohn, Weirich: Cold gas spraying of nickel-titanium coatings for protection against cavitation. Journal of Thermal Spray Technology, 30, 2021, 131.
5. Boulos: RF induction plasma spraying: state-of-the-art review. Journal of Thermal Spray Technolpogy, 1, 1992, 33.
6. Samal, Tyc, Cizek, Klecka, Lukac, Molnarova, de Prado, Weiss, Kopecek, Heller, Sittner, Chraska: Fabrication of Thermal Plasma Sprayed NiTi Coatings Possessing Functional Properties. Coatings, 11, 2021, 610.

Jméno a pracoviště vedoucí(ho) bakalářské práce:

doc. Ing. Jan Čížek, Ph.D. Ústav materiálového inženýrství

Jméno a pracoviště druhé(ho) vedoucí(ho) nebo konzultanta(ky) bakalářské práce:

Datum zadání bakalářské práce: **23.03.2023** Termín odevzdání bakalářské práce: **31.07.2023**

Platnost zadání bakalářské práce: _____

doc. Ing. Jan Čížek, Ph.D. podpis vedoucí(ho) práce	doc. Ing. Ladislav Cvrček, Ph.D. podpis vedoucí(ho) ústavu/katedry	doc. Ing. Miroslav Španiel, CSc. podpis děkana(ky)

III. PŘEVZETÍ ZADÁNÍ

Student bere na vědomí, že je povinen vypracovat bakalářskou práci samostatně, bez cizí pomoci, s výjimkou poskytnutých konzultací. Seznam použité literatury, jiných pramenů a jmen konzultantů je třeba uvést v bakalářské práci.

. _____
Datum převzetí zadání

_____
Podpis studenta

Statement

I declare that I have prepared my bachelor thesis independently, and exclusively using the sources and literature listed in the list of cited literature.

In Prague: ……

……

Signature:

Acknowledgments

I would like to thank Assoc. prof. Jan Čížek, Ph.D. for supervising this Bachelor's thesis, valuable advice, guidance in its writing and help with the experimental part. I would also like to thank colleagues from the Institute of Plasma Physics of the Czech Academy of Sciences, Ing. Jakub Klečka for his help with the sample preparation, RNDr. František Lukáč, Ph.D. for help with the XRD analysis, and Mr. Stanislav Lambert for help with the PSA analysis.

Anotace

Autor:	Tomáš Heller
Název:	Slitina NiTi připravená technologií studené kinetizace
Rozsah práce:	41 str., 14 obr., 3 tab.
Akademický rok:	2022/2023
Škola:	ČVUT v Praze, Fakulta strojní
Ústav:	Ú12132 – Ústav materiálového inženýrství
Vedoucí diplomové práce:	doc. Ing. Jan Čížek, Ph.D.
Klíčová slova:	Studená kinetizace, slitina NiTi, charakterizace materiálů, nástřiky
Abstrakt:	Tato práce se zabývá slitinou NiTi vyrobenou metodou studené kinetizace. Teoretická část práce popisuje principy, vlastnosti a aplikace metody studené kinetizace a dále slitiny NiTi. V experimentální části práce je poté charakterizován vstupní prášek pomocí metod SEM, EDX, XRD a analýzy velikosti částic. Zjištění odhalují nepravidelnou morfologii směsi prášku s částicemi titanu a niklu. V práci je dále připraven a charakterizován odpovídající nástřik, který je hutný a s dobrým rozhraním s podkladem, leč nehomogenní z hlediska chemického a fázového složení, což je právě dáno charakterem vstupního prášku.

Annotation

Author:	Tomáš Heller
Title:	NiTi alloy produced by cold spray
Extent of the thesis:	41 p., 14 fig., 3 tab.
Academical year:	2022/2023
University:	CTU in Prague – Faculty of Mechanical Engineering
Department:	Ú12132 – The Department of Materials Engineering
Thesis supervisor:	doc. Ing. Jan Čížek, Ph.D.

Keywords:	Cold spray, NiTi alloy, materials characterization, coatings

Abstract:	This thesis investigates the NiTi alloy produced by cold spray. The theoretical part of the thesis describes the principles, properties and applications of the cold spray and the NiTi alloy. The experimental part of the thesis then characterizes the starting powder by SEM, EDX, XRD and particle size analysis. The findings reveal an irregular morphology of the powder mixture with titanium and nickel particles. The corresponding coating is then prepared and characterized, which is dense and with good interface with the substrate, but inhomogeneous in terms of chemical and phase composition, which is precisely due to the nature of the feedstock powder.

Contents

List of used symbols and abbreviations

A_f	Austenite finish temperature
A_s	Austenite start temperature
M_d	Martensite deformation temperature
M_f	Martensite finish temperature
M_s	Martensite start temperature
v_{cr}	Critical velocity
η	Normalized impact velocity

ASI	Adiabatic shear instability
CS	Cold spray
CSAM	Cold spray additive manufacturing
CTE	Coefficient of thermal expansion
DE	Deposition efficiency
EDX	Energy dispersive X-ray spectroscopy
MT	Martensitic transformation
PSA	Particle size analysis
RT	Reverse transformation
SE	Superelasticity
SEM	Scanning electron microscopy
SMA	Shape memory alloys
SME	Shape memory effect
TS	Thermal spray
XRD	X-ray diffraction

1 Introduction

NiTi alloys are widely known for their shape memory and superelasticity. In addition, they however also possess high corrosion and wear resistance and hardness, which predispose them for many applications, for example in medicine. Here, manufacturing entire complex parts made of NiTi may be complicated and expensive. However, they can be used in a form of surface coatings for other materials. Cold spray is a technique that can readily deposit relatively thick NiTi coatings. It is similar to thermal spray methods, but without many of their disadvantages due to its solid-state process character.

This thesis is a pioneering part of an experimental study, aiming at fabrication of functional NiTi coatings by the cold spray technology.

The objective of the theoretical part of this thesis is to introduce the reader to the principles, properties, and applications of cold spray, as well as the properties and applications of the NiTi alloy.

The goal of the experimental part of this thesis is to characterize the feedstock powder and the resulting coating produced by cold spray. The morphology of the powder and coating are characterized using scanning electron microscopy. Subsequently, their chemical composition is analyzed using energy-dispersive X-ray spectroscopy, and the phase composition is examined using X-ray diffraction. Furthermore, the particle size distribution of the powder is also analyzed.

2 Literature review

2.1 Cold gas dynamic spraying

2.1.1 Introducing CS

Cold gas dynamic spraying (CGDS, often shortened to cold spray, CS) is a method of high-velocity powder spraying for the purpose of creating compact coatings on solid substrates. It is related to thermal spray methods. However, as opposed to them, the sprayed powder is not supplied thermal, but rather kinetic energy: in thermal spraying, the powder particles are heated beyond their melting temperature, while in cold spray, the temperature always remains lower than the melting point of the material. The lack of thermal energy is compensated by the high velocity - the powder is accelerated by the means of a propellant gas to a supersonic velocity (up to 1200 m/s). When an accelerated powder particle hits the substrate, its kinetic energy is transformed into thermal energy and severe plastic deformation. Through it, the particle is firmly bonded to either the substrate or previously sprayed layers [1], [2].

The cold spray method can be used to deposit many kinds of materials, but by far the most frequent are metals and alloys. Cold spraying of pure ceramics is only possible with special CS powders or using related methods such as aerosol deposition [3]. On the other hand, spraying of composites which have a deformable component (usually a metal or less frequently a polymer) is possible [4]. In metals, the suitability for deposition is proportional to the plastic deformability of the materials. Thus, best suited for CS are metals with face-centered cubic (FCC) crystal lattice such as copper, aluminum, nickel, gold, silver or γ-iron. Hexagonal close-packed (HCP) and body-centered cubic (BCC) metals such as titanium, magnesium or chromium have a lower number of sliding planes, resulting in lower deformability and thus being more difficult to deposit [5], [6].

Cold spray not only allows spraying of a coating material dissimilar to that of the substrate, but also allows the coating to be composed of various materials, enabling formation of mixed, multilayered, or graded coatings [4].

Originally, cold spray was investigated as a method for surface coatings preparation (similar to high temperature thermal spray methods). Given its versatility, it has since been developed for other uses:

1. Surface coatings
2. Additive manufacturing
3. Repairs or restorations
4. Studying materials behavior [4], [5]

As opposed to the high temperature thermal spray processes, there is virtually no limit in the thickness of the CS coatings. This enables using CS for additive manufacturing production. Cold spray additive manufacturing is used both for rapid prototyping and for manufacturing of functional components. Using robotic systems, it is possible to create even complex-shaped parts (examples of possible uses of cold spray additive manufacturing, CSAM, include parts such as rocket nozzle, see Fig. 1). CS is often used as a first step of manufacturing, followed by machining of the part to final dimensions and heat treatment to improve ductility [4], [5].

Fig. 1 - Rocket nozzle produced by cold spray additive manufacturing [7].

The second benefit of CS is its superior adhesion to the substrate. This allows using cold spray for repairing or restoration of damaged components. This represents an economic route, since replacing a component is often expensive and may also be time consuming due to typical lead times of advanced components. The dimensional loss due to damage can be restored with cold spray and the repaired part then machined back to original dimensions. Further, low-pressure cold spray systems have the advantage of being portable, thus enabling in situ repairs [5].

Lastly, the principles of cold spray may be used to study behavior of materials subjected to extremely high strain rates, not easily reachable by other processes, as suggested by Asadi et al. [4].

2.1.2 Principles

The principle of cold spraying is formation of a compact material by depositing and stacking individual powder particles upon their impact at a substrate. This is achieved by the following process.

In a CS system, the powder is accelerated in a de Laval nozzle by a propellant gas. There are two main types of CS systems: low-pressure and high-pressure. In high-pressure CS systems, the powder is injected into the gas flow before the nozzle at a high pressure. In such configuration, the gas flow is separated into two parts: the main part flows through the gas heater and into the nozzle, while the auxiliary part of the gas is led through the powder feeder and into the nozzle by a separate inlet. In low-pressure cold spray systems, the powder is introduced into the stream later, at the diverging part of the nozzle at a lower (atmospheric) pressure. Both systems are schematically shown in Fig. 2 [2], [4], [8].

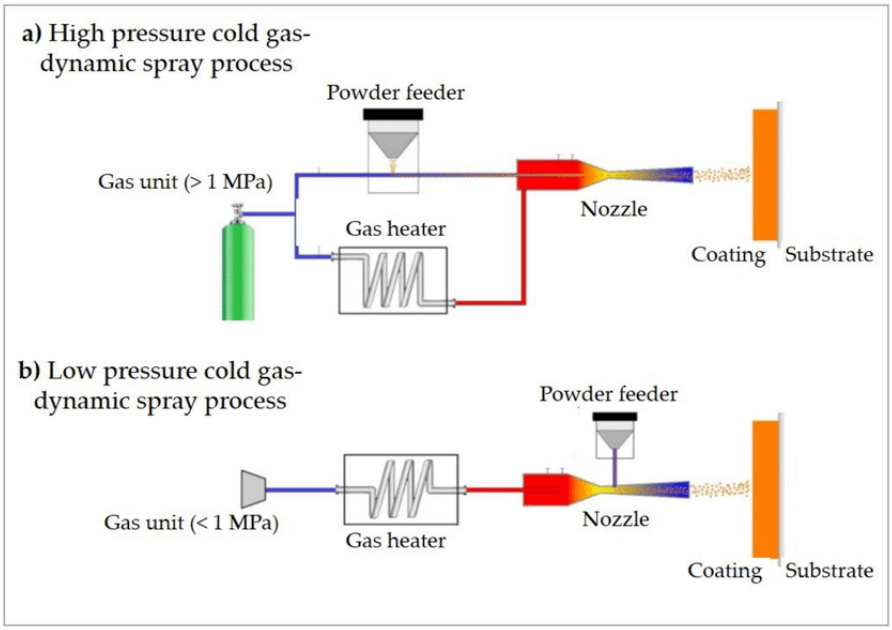

Fig. 2 - Schematic comparison of high-pressure and low-pressure CS systems [8].

Although the process is called "cold gas dynamic spray", the gas is heated. As opposed to the high temperature thermal spray process, this is not done to melt the powder particles. Instead, it is done to reach higher velocity of the gas in the nozzle and thus achieve higher particle velocity. In other words, even though the temperature of the gas can be higher than the melting point of some sprayed materials, the powder particles reach significantly lower temperatures due to the gas cooling rapidly during its expansion after exiting the nozzle, as well as due to the extremely short dwell times within the gas jet [2], [8].

In flight, the particles need to achieve a velocity that lies within a certain range to allow them to successfully bond upon impact. The lower bound of this range is the so-called critical velocity, the lowest possible velocity for a successful bonding. With increasing velocity, the deposition efficiency (DE, the ratio of successfully bonded particles to the number of sprayed particles) increases up to a saturation level. If the velocity is even higher, DE starts to decrease due to erosive effects of the impinging particles and eventually reaches 0% where the second critical, so-called erosion velocity is defined. The window of deposition of each material lies between the critical velocity and the erosion velocity, with optimum velocity being the velocity of DE saturation [1], [2].

The critical velocity is a very important parameter of the cold spraying process. Its value depends on many factors, mainly on the materials of the feedstock powder and the substrate. Other factors include temperature of the impinging particles and their size, and surface oxidation of both the particles and the substrate [4]. In the paper by Schmidt et al. [2], the critical velocity has been determined as a global parameter of the whole process by defining it as the velocity at which the cold spray process has DE of 50%. Later the critical velocity of a single particle has been estimated both experimentally and by numerical simulations [4], [9].

For identical materials of the coating and the substrate, a formula was proposed to determine the critical velocity:

$$v_{cr} = \sqrt{\frac{A\sigma}{\rho} + B c_p (T_m - T_p)}, \tag{2.1}$$

where T_m denotes the melting temperature of the materials, T_p is the mean particle temperature upon impact, c_p is the heat capacity of the material, ρ is density of the material and σ is the temperature-dependent flow stress. The values of the constants A and B have been determined to be $A = 4$ and $B = 0{,}25$ for a typical particle size distribution [2], [4].

During the impact, the kinetic energy of the particles is converted into heat and visco-plastic deformation. The deformation causes work hardening, while the heat generation causes thermal softening. At a certain point, the thermal softening dominates over the work hardening, leading to very high localized strain rates and to a so-called adiabatic shear instability (ASI), which causes jetting of the materials at the interface [3]. The jetting breaks up and removes the inevitable surface oxides and thus enables intimate contact of clean metallic surfaces. This intimate contact results in a metallurgical bonding of the two, occurring at the rim of the contact zone first. With increasing impact speed, the fraction of the bonded area gets larger, although it never covers the entire contact zone as the very “south pole” of the particle may not get bonded. This is because the oxides at the center of impact are not broken up and removed by

the jetting [4], [10]. An example of a successfully bonded cold sprayed particle is shown in Fig. 3.

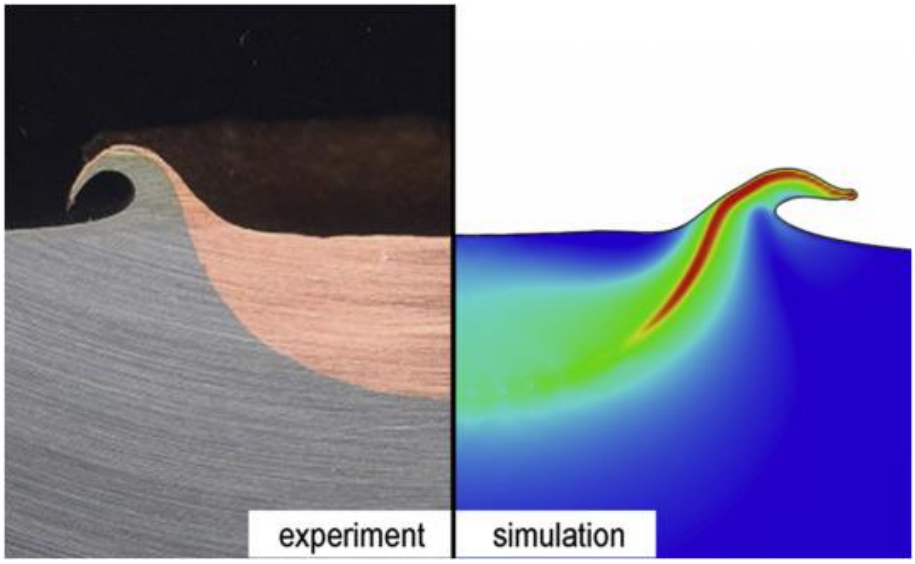

Fig. 3 - Large-scale impact of a copper ball onto a steel surface (experimental and numerical simulation) [4].

The metallurgical bonding in CS is complemented by mechanical interlocking (magnified to vortex-like intermixing of the two materials in some cases). Mechanical interlocking is a mechanism encountered in high temperature thermal spray processes (where it is frequently the only bonding mechanism) and results from the particles conformation to the surface asperities, providing additional adhesive/cohesive strength [11], [12].

2.1.3 Properties of CS deposits

The properties of cold sprayed deposits are dictated by the processes that take place during the impact of the powder particles. The severe plastic deformation leads to grain refinement and work hardening through a formation of a large number of lattice defects (most prominent being dislocations). The microstructure is typically also highly anisotropic as a result of the spraying principles [4].

The mechanical properties of the deposit are similar to mechanical properties of a highly cold-worked bulk material. These include low ductility and elongation to failure, high yield strength and high hardness. There is a partial correlation

between these properties and the normalized impact velocity $\eta = \frac{v}{v_{cr}}$ [4]. In other words, the excess of kinetic energy enables an increased bonding and increases the work hardening [2]. The ductility of the deposits can be improved, e.g., by annealing [8].

While the coatings made by cold spraying have minimal porosity, there are some imperfections in the form of partially unbonded interfaces (see section 2.1.2). These may act as crack nuclei under conditions of tensile loading and thus, e.g., diminish the adhesive and cohesive strength of the coatings. Nevertheless, the adhesive strength is typically an order of magnitude higher than that of the high temperature thermal spray processes, reaching up to 120 MPa (or even 200 MPa under special conditions) [4].

The high density of lattice defects also limits electron mobility. This naturally leads to a decrease in electrical conductivity, which is about 80% of the electrical conductivity of the bulk material [2], [4].

2.1.4 Comparison to thermal spraying

Cold spraying can be best compared to thermal spraying, as their basic principles are somewhat similar [5], [4].

The main difference between CS and thermal spray (TS) is that the powder particles do not melt and are deposited in their solid state at a lower temperature. This triggers several advantages of the CS deposits over the TS counterparts, such as retainment of chemical and phase composition (including absence of oxidation), lower porosity, and more favorable residual stresses [1], [8].

Due to the need for melting and subsequent solidification and the potential selective deposition, the chemical and phase composition of thermal spray deposits may be different from the composition of the feedstock. High temperatures also lead to oxidation and consequently to a high amount of oxides in the deposits (sometimes more than 1.5 wt.% for sensitive metals). In CS

deposits, the chemical and phase composition as well as the amount of oxides remain identical to the feedstock [4], [8].

The supersonic CS deposition also prevents formation of a large number of pores. And even then, the pores that actually do form tend to be closed by the shot-peening effect resulting from impacts of particles forming the subsequent layers. That way, the porosity can reach as low as 0.01%, i.e., a near theoretical density [4], [8].

The shot-peening effect of CS also results in a formation of residual stresses in the sprayed materials. In high temperature thermally sprayed coatings, these residual stresses are generally tensile, as a result of a significant dimension change during cooling of the sprayed layers, and CTE mismatch to the substrate. Further, these tensile stresses increase with increasing thickness of the coating, thereby limiting the maximum achievable thickness. As opposed to these, the residual stresses in CS are compressive. This is beneficial as, for instance, there is no thickness limit, enabling CS to be used as a method for additive manufacturing [5], [8].

2.2 Shape memory alloys

2.2.1 Introduction to shape memory alloys

Shape memory alloys (often shortened to SMA) are a class of metallic compounds which exhibit the ability to "memorize" their shape and return to it when subjected to suitable stimuli. There are two types of shape memory alloys based on the type of stimulus needed: thermal SMA and magnetic SMA. Thermal SMA return to their shape when heated above a certain temperature, while magnetic SMA respond to magnetic fields. The focus in this thesis will be on the thermal shape memory alloys [13], [14].

Due to their favorable mechanical properties, the most widely used SMA in this group are NiTi, first reported by Buehler et al. in [15], but many other types of alloys exist and are used. These include Fe-based (Fe-Mn-Si), copper-based (Cu-

Zn-Al, Cu-Al-Ni), as well as Ag-, Co- and Au-based alloys (Au-Cd alloy was the first discovered to exhibit the shape memory) [14].

2.2.2 Principles

The shape memory alloys exhibit two phenomena: the shape memory and superelasticity. Both phenomena are based on martensitic transformation (MT) from a parent phase (austenite) and the reverse transformation (RT) from martensite back to austenite (both are diffusion-less solid phase transitions). The parent phase has a cubic structure, while the martensite has a structure with a lower symmetry (monoclinic in NiTi systems) [13].

At higher temperatures, the material is composed of austenite. Upon cooling, the MT commences at a certain temperature, denoted as M_s (martensite start). With further cooling, the transformation ends at temperature M_f (martensite finish). If such sample is heated, the RT starts at temperature A_s (austenite start, $A_s > M_s$) and finishes at A_f (austenite finish) [13], [16].
The fifth important temperature is the martensite deformation temperature, M_d, which is generally higher than A_f. If the austenitic phase is externally loaded while in the temperature range between A_f and M_d, it transforms into detwinned martensite and can deform elastically to a large strain. If it is loaded while at a higher temperature, it deforms in the same manner as other metals, without transforming into martensite [14].

The exact temperatures depend on the composition of the alloy and can be finely tuned (for example by varying nickel content in the NiTi systems) [14], [13].

The mechanism of shape memory (SME) is following: a sample of given shape is cooled below M_f and thus undergoes martensitic transformation. Its structure becomes a twinned martensite and the macroscopic shape does not change. Under external loading, the twin boundaries move, which results in a macroscopic shape change. The loading needs to be low enough not to cause critical shear stress which would lead to a permanent deformation. This also puts a bound on fully recoverable strain. If the sample is deformed to the maximum recoverable strain, the martensite becomes fully detwinned. When the external

forces are then removed, the sample remains in its deformed shape. If it is then heated, the RT takes place. The structure reverts back to austenite and the shape reverts back to the original, undeformed shape [13], [14], [16].

Superelasticity (SE) takes place only if the structure is austenitic and can undergo stress-induced MT (the temperature is between A_f and M_d). In such case, the external loading causes stresses in the sample that induce the martensitic transformation into a detwinned martensite. This manifests macroscopically as an elastic deformation with a large recoverable strain (again restricted by the fact that external loading cannot cause stress higher than the critical shear stress). When the external loading is removed, the material structure transforms back into austenite, thereby restoring its original shape [13], [14].

The dependence of crystal structure on the temperature, stress and strain is shown schematically in Fig. 4 [14].

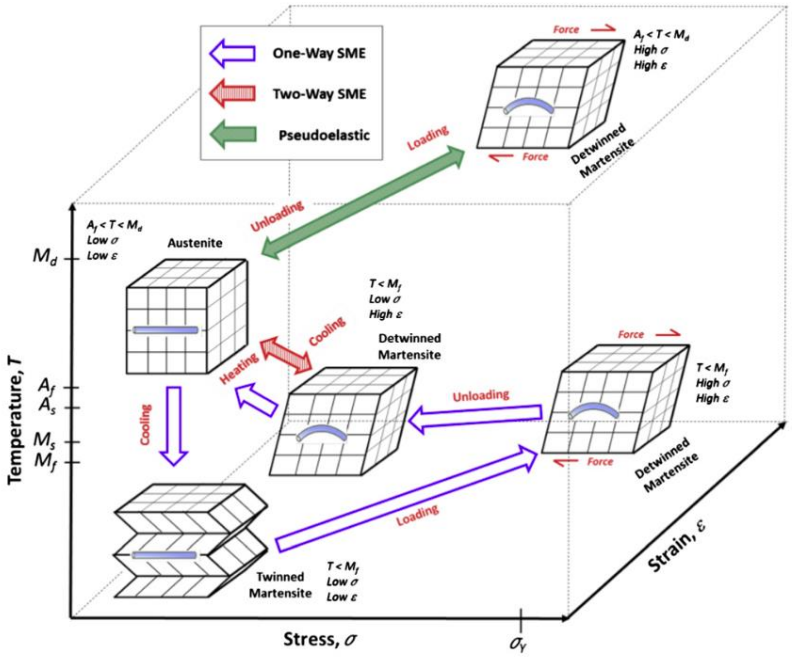

Fig. 4 - SMA phases and crystal structures [14].

The recoverable strain for both SME and SE depends on the properties of the alloy but is generally higher than what is achievable by common alloys (about 4–5% for Cu-based alloys and approximately 8.5% for NiTi alloys) [14].

In addition, a material can also have a two-way shape memory, if it is "trained" to remember its shape at both high and low temperatures (i.e., both in austenitic and martensitic state). Depending on whether the sample is cooled or heated, it can change shape in one direction or the other. Commercially, two-way shape memory is less used due to the need for the training and due to usually only producing about half of the recovery strain of one-way shape memory for the same material [13], [14].

2.2.3 Applications

The applications of shape memory alloys can be generally divided into four categories:

1. Free recovery applications
2. Constrained recovery applications
3. Work production applications (actuators)
4. Superelastic applications

In the free recovery applications, the desired function of the memory element is simply to return to its original shape. Conversely, in the constrained recovery applications, the element is prevented from changing shape and thus produces a force acting on the constraining element (SMA can generate stresses up to 700 MPa in this way) [13], [14].

In work-producing applications, the SMA element changes shape while under external loading. The motion of the element against the loading produces work (this application thus falls between the free recovery with no forces generated and the constrained recovery with no shape change) [13], [14].

In superelastic applications, the desired effect is superelasticity instead of shape memory. These applications may involve potential energy storage, vibration dampening or structure reinforcement [13], [14].

Two areas in which SMA have a large number of commercial applications are medicine and actuators [13].

NiTi alloys are often used in medicine thanks to their corrosion resistance, as well as biofunctionality and biocompatibility. Both SME and SE are used, SME in dental implants or in orthopedy and SE for example in dental arch wires [13].

Shape memory actuators transform thermal energy into mechanical energy, generating force and motion. Such actuators have several advantages over conventional actuators, such as being significantly smaller and far simpler mechanically (as they react to environmental stimuli directly). Depending on their configuration, simple SMA actuators can generate not only linear or circular motion, but also complex 3D motions. However, there are also some disadvantages: the most prominent one is that the system reacts to heat transfer and thus the reaction times are longer. SMA actuators are thus best suited to application where a significant displacement or force is needed, with no requirements for a short response time [13], [14].

Although the Cu-based SMA are generally cheaper and can transform at higher temperatures (up to 200 °C), the NiTi alloys are used more often as they have more favorable properties. These include lower brittleness and higher stability and fatigue strength as well as work density (in the range of 10 J/cm^3) [14].

2.3 Experimental analysis techniques

Several methods of analysis were used in the experimental part of this thesis. In this section, a brief theoretical description of these methods is provided.

2.3.1 Scanning electron microscopy (SEM)

Electron microscopy is used to examine samples at magnifications unreachable by light microscopes. In scanning electron microscopy, a beam of electrons focused by magnetic lenses scans the surface of the sample. This triggers a range of responses from the sample material that can be captured and analyzed. Most often, secondary electron detection and backscattered electron detection are used. Secondary electrons are emitted due to scattering interaction with incoming electrons from the beam. These electrons have low energy and can thus originate from depths of at most several nanometers below the surface.

Backscattered electrons are electrons from the initial electron beam that are reflected by the sample during scattering interaction with the surface atoms. These electrons have a higher energy than the secondary electrons. More electrons are backscattered by heavier elements and can thus be used to contrast between different chemical compositions [17].

2.3.2 Energy dispersive scanning spectroscopy (EDX)

EDX is a method used to determine the chemical composition of a given sample. To measure the composition, electrons of the surface atoms of the sample are excited and thus dislodged from its shell. Another electron from a higher energy shell then fills the gap, reducing its excess energy in the form of emitted X-rays. The energy of the X-ray that can be captured is specific to a certain element, thus revealing chemical composition of the sample [18].

2.3.3 X-ray diffraction (XRD)

This method is used to determine phase composition of a sample. X-ray radiation is directed at the sample where scattering occurs, with atoms in the crystal lattice acting as 3-dimensional diffraction grating. The scattered electromagnetic waves then interfere. This interference is mostly destructive - it is constructive only under conditions given by Bragg's Law:

$$n\lambda = 2d \sin\theta \tag{3.1}$$

where n is the diffraction order (n = 1, 2, 3, ...), λ is the wavelength of the X-ray radiation, d is the lattice parameter of the analyzed crystal and θ is the angle of incidence of the X-rays [19]. The diffraction pattern is measured by a detector and then compared to a database to check for a correspondence to known patterns. In a diffractometer, the angle θ between the X-ray beam and the sample changes while a detector rotates on an arm at angle 2θ.

2.3.4 Laser diffraction particle size analysis

This method uses diffraction of laser beams on the powder particles to measure the particle size distribution. Particles either in a liquid suspension or dispersed in air are passed through a laser beam. Due to the diffraction, the angle of the beam is changed. Here, large particles cause small angular changes, whereas

small particles cause large changes. The laser beam then passes through a lens where it is focused into a detector array. From the detected angular changes, the particle size distribution is calculated [20].

3 Experimental setup

The goal of this section is to describe the used powder and substrate materials, the cold spray deposition process details, and the details of the analytical methods used for characterization of the feedstock NiTi powder as well as the corresponding coating. The phase composition of the powder was analyzed using X-ray diffraction and its size particle distribution using laser diffraction analysis. The microstructure of both the powder and the coating was characterized using scanning electron microscopy, while their chemical composition was determined using energy dispersive X-ray spectroscopy.

3.1 Materials

The substrate used was a pure Al tube of a 30 mm diameter (see Fig. 5). Such choice of the substrate material allows for an easy determination of the coating-substrate interface, while the geometry allows for an easy determination of the cold spray process deposition efficiency, and, at the same time, saves the feedstock powder by limiting geometrical over-spraying. The surface of the substrate was not polished, or grit blasted prior to deposition.

Fig. 5 - Aluminum tube substrate with cold sprayed NiTi coating.

According to the manufacturer (American Elements, USA), the used powder was a NiTi alloy powder of 50:50 at.% composition, with 99.9% purity and -325 mesh

size (i.e., below 44 μm). For microscopic observation of the powder morphology, a sample was prepared by pouring the particles onto conductive adhesive carbon tape. This was done without applying external pressure in order not to alter or damage the original particle morphology. The powder was then observed and characterized using SEM and EDX methods.

For this thesis, scanning electron microscope EVO MA 15 (Carl Zeiss SMT, Germany) with LaB_6 cathode as a source of electrons was used to assess the structure of the powder. An acceleration voltage of 20 kV was used, and the samples were observed in low-vacuum mode at 30 Pa of nitrogen gas introduced into the chamber to prevent excessive charging of the samples. The images were collected in backscattered electrons mode at relatively short work distances of 8–10 mm. Using this setup, the chemical heterogeneity is pronounced and easier to comprehend.

For the EDX analysis, Quantax (Bruker, Germany) SDD detector XFlash® 5010 was used. The overall chemical composition of the powder was determined from a large area at low magnification to enhance the statistical reliability, as well as from localized regions to comprehend potential local inhomogeneities. An enhanced EDX mapping was further carried out to visualize the element distribution in the powder.

The sample for X-ray diffraction analysis was prepared by pouring the powder into a holder which was then placed into the diffractometer chamber. The XRD analysis was done using D8 Discover (Bruker, Germany) diffractometer with Cu anode and 1D detector LynxEye. The range of 2θ was selected as 15°–160°, and the total time in each step was 192 s. The measured spectra were compared to a database and the quantification of phases according to the Rietveld method was carried out using Topaz software. This method served to determine phase composition of the powder, complementing the data from the EDX analysis.

For the particle size analysis, the powder particles were suspended in demineralized water and placed into Mastersizer 3000 particle size analyzer (Malvern, UK). The detectable range was set to 0.01–10000 μm and both

numerical as well as volume distribution data were collected along with their cumulative counterparts. To further help in our understanding of the powder character, the measurements were repeated twice: with and without ultrasonic function. The ultrasonic vibrations could, for loosely agglomerated powders, trigger the agglomerate particles separation, a difference that would be detected in the obtained distribution curves.

3.2 Deposition and characterization of the coating

The NiTi coating was deposited using a commercial Impact Spray System 5/11 (Impact Innovations, Germany). Due to the lack of available literature sources on deposition of NiTi, the used process parameters were based on the average between Ni and Ti: gas temperature 1100 °C, gas pressure 5 MPa with nitrogen used as the process gas.

From the coated 30-mm Al tube, a sample was cut using a high-speed precision saw Secotom-50 (Struers, Denmark) and embedded in an epoxy resin. After the resin cured, the sample was ground and polished using automated polisher Tegramin 25 (Struers, Denmark). First, the sample was ground using SiC #320 paper, followed by Largo grinding surface with DiaPro 9 µm diamond suspension. The sample was then polished using Dur polishing cloth with DP 3 µm diamond suspension followed by Nap polishing cloth with DP 1 µm. The final step was polishing with Chem polishing cloth using OP-S colloidal silica suspension.

The prepared metallographic coating cross-section was observed and characterized using SEM, EDX and XRD methods. The characterization was done using the same equipment and parameters as the NiTi feedstock powder.

4 Results and discussion

4.1 Powder

Micrographs of the NiTi powder were taken from two different areas at successively higher magnifications from 100× to 5000×. The morphology of the powder is shown in Fig. 6.

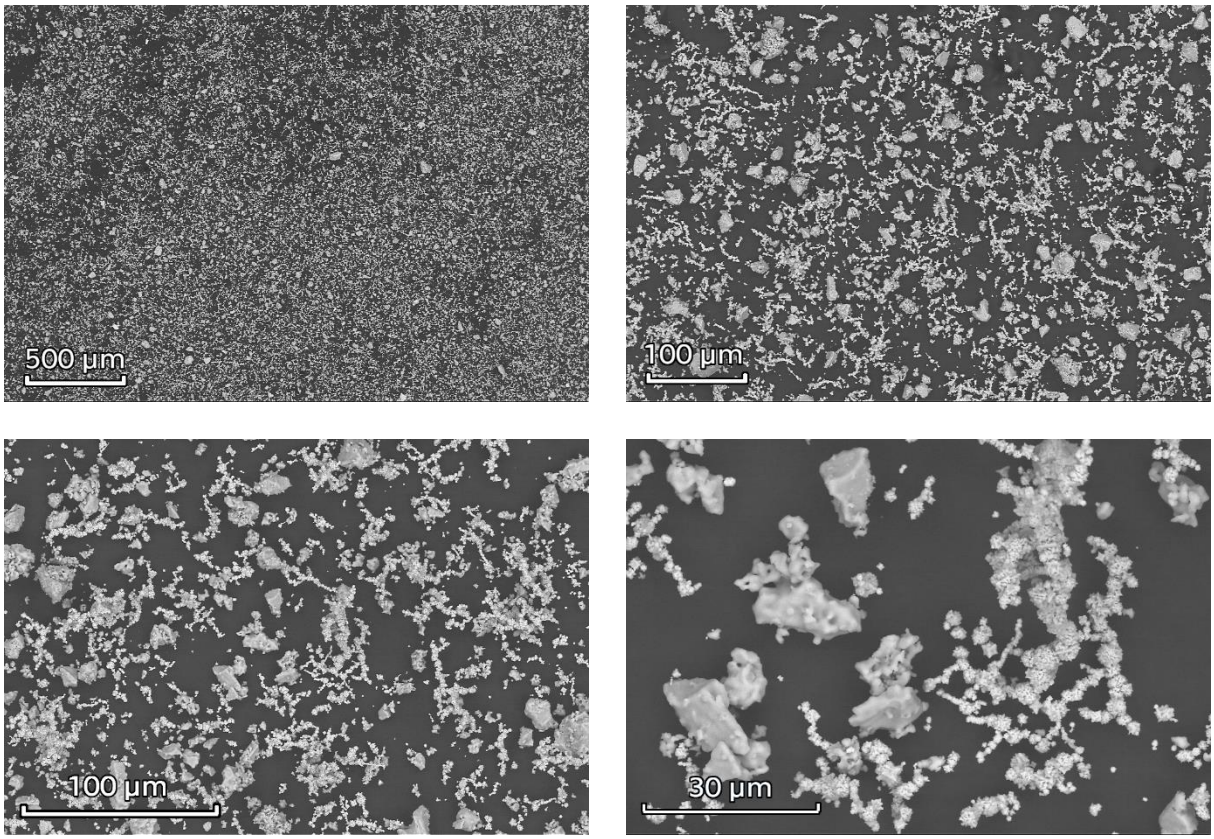

Fig. 6 - Morphology of the feedstock NiTi powder at various magnifications.

These SEM images show that the powder particles are not spherical and in fact have a very irregular shape. Further, the powder is composed of two dissimilar types of particles: significantly larger, more regular particles, and long, chain-like thin particles which seem to be aggregates of many smaller ones.

The surface of either type of particles is not smooth. The larger particles are rough and seem to be covered by smaller satellites. The thin particles appear to be composed of mutually linked, much smaller particles, creating irregular complex chains with limited branching. A certain proportion of the small particles seems

to have broken off from the chains. Both types of particles are shown side to side in a higher detail in Fig. 7.

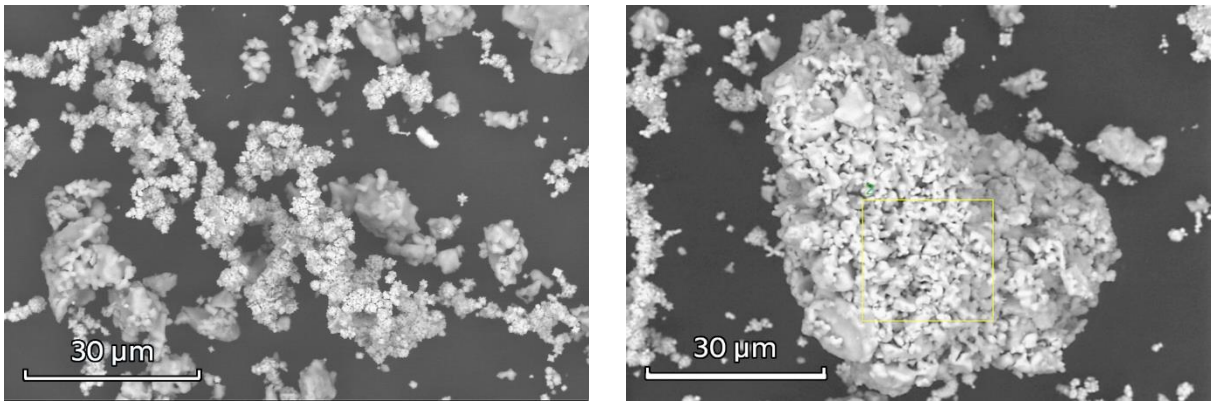

Fig. 7 - Morphology of the two different particle types in the feedstock NiTi powder at 3000× magnifications.

The reason of the dissimilar particle morphology was disclosed using the EDX method. As can be seen from the EDX elemental mapping in Fig. 8, each type of particle has a different composition. The more regular, larger particles are composed of titanium, while the chain-like particles are composed of nickel. In other words, the information from the powder manufacturer on the powder being an alloy was not correct. Instead, the powder was a mere blend of two pure powders, Ni and Ti.

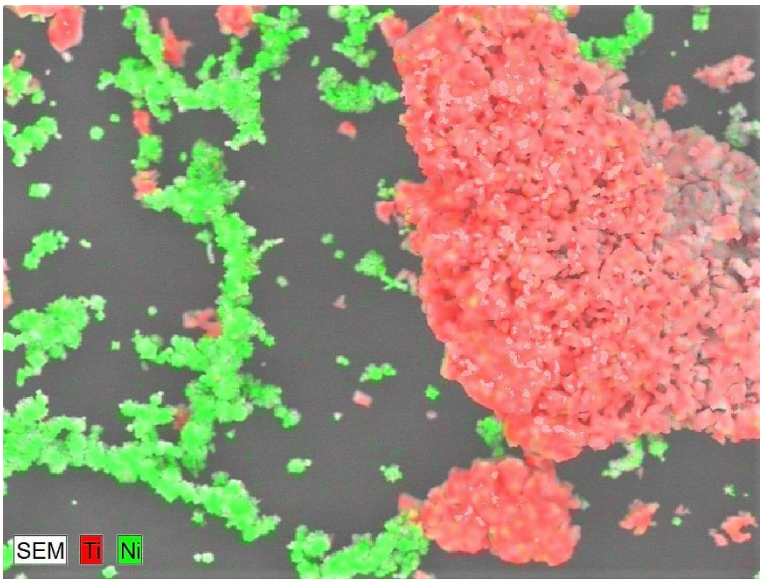

Fig. 8 – Elemental mapping of the feedstock NiTi powder.

In addition to qualitative elemental mapping, the chemical composition data were obtained as quantitative area analysis as well. These data were then compared to the data provided by the manufacturer, 50:50 at.% (corresponds to 44.9 wt.% Ti and 55.1 wt.% Ni). The comparison of the EDX data with those provided by the manufacturer and those obtained by the XRD analysis are shown in Table 1. The actual chemical composition of the powder does not agree with the declared composition, with significantly more titanium present. This is critical toward the intended use for SMA applications as even a relatively slight deviation of the composition from the optimum yields a considerable decrease in the SMA effect strength.

To complement the data from EDX, the XRD analysis was done. The resulting diffraction spectrum is shown in Fig. 9. The analysis showed that in addition to titanium and nickel, titanium hydride was present in the composition in an amount of 8.2 wt.%. This may be a residue from the production of the powder, given the affinity/reactivity of titanium to/with hydrogen [21].

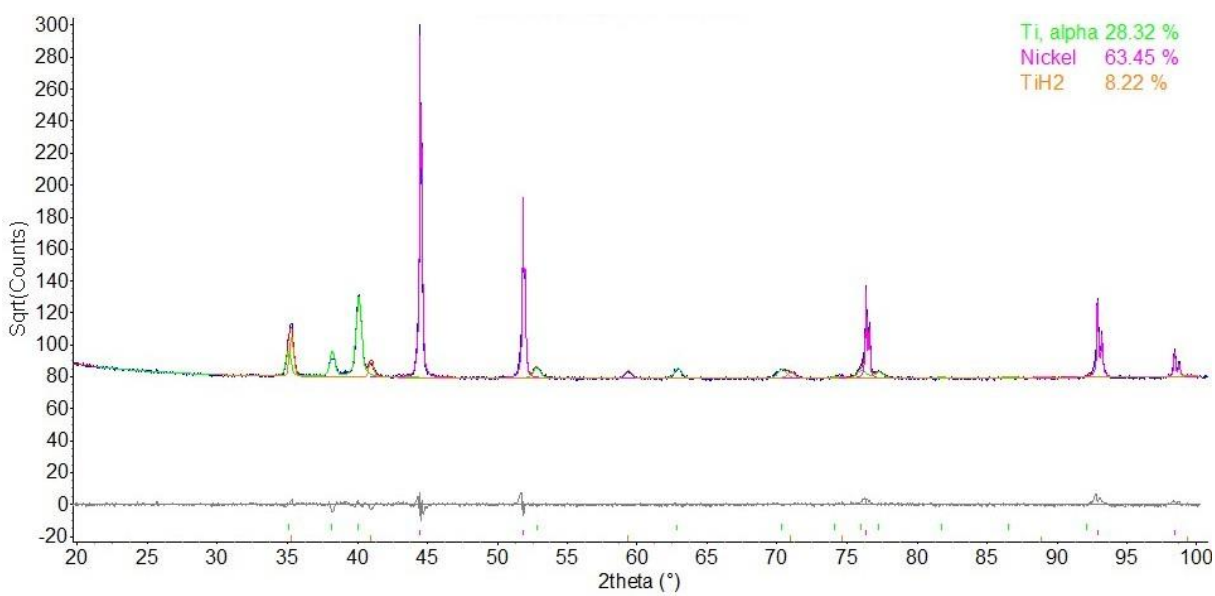

Fig. 9 – XRD diffraction spectrum of the powder.

Even when considering the fact that hydrogen could not be detected by EDX, these results still differ significantly from the results from EDX analysis, and the data provided by the manufacturer. The XRD measurements were repeated, but the results remained virtually the same. The reason for this significant difference

in composition is not clear at the time of writing and is currently being investigated.

Table 1 - Comparison of the powder composition data

Source	Ti (wt.%)	Ni (wt.%)	TiH_2 (wt.%)
Manufacturer	44.9	55.1	-
EDX powder	54.1	45.9	-
XRD powder	28.3	63.5	8.2

For particle size analysis, four particle size distribution curves were obtained by the laser diffraction analysis, corresponding to the combinations of the number density measurement vs. the volume density measurement, and regular measurement vs. the measurement including ultrasonic vibrations.

All the data was measured with a weighted residual under 1%, showing a good fit of the calculated output to the measurement data.

The measured distribution curves are shown in Fig. 10 for number density and in Fig. 11 for volume density. In these figures, the red curves represent the density measured without ultrasound and blue curves represent density measured including ultrasound, while the solid lines represent the measured particular density, and the dashed lines represent the respective cumulative density.

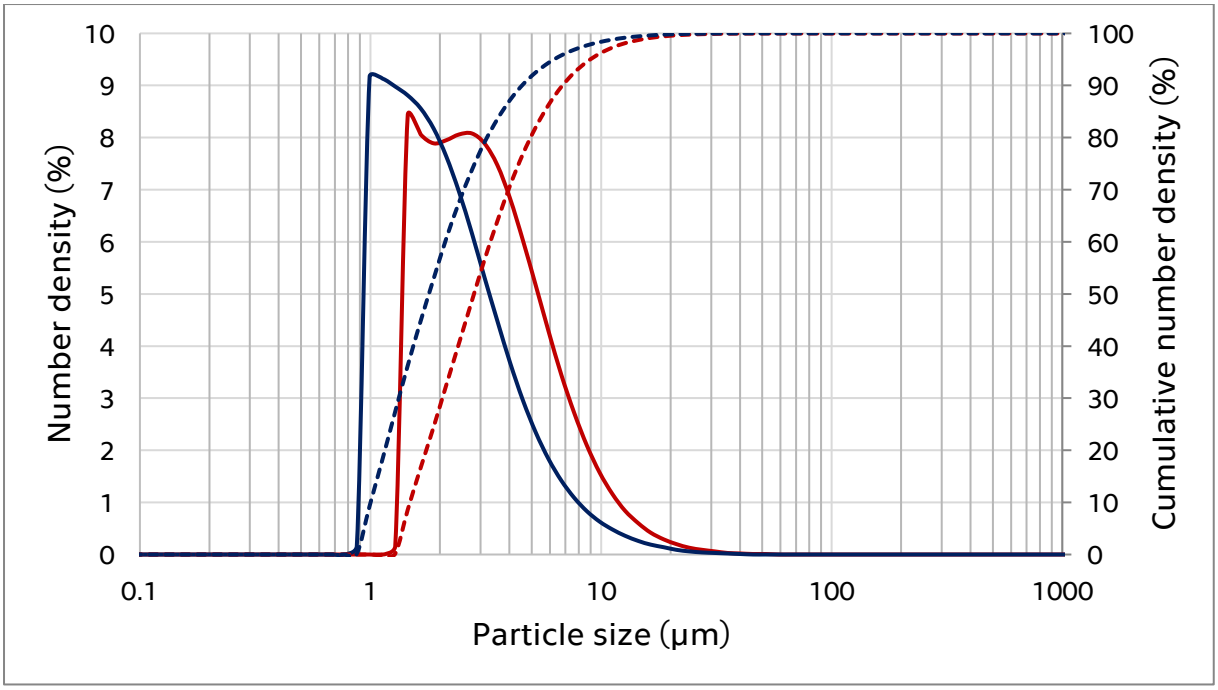

Fig. 10 – Number distribution of the feedstock NiTi powder particle sizes.

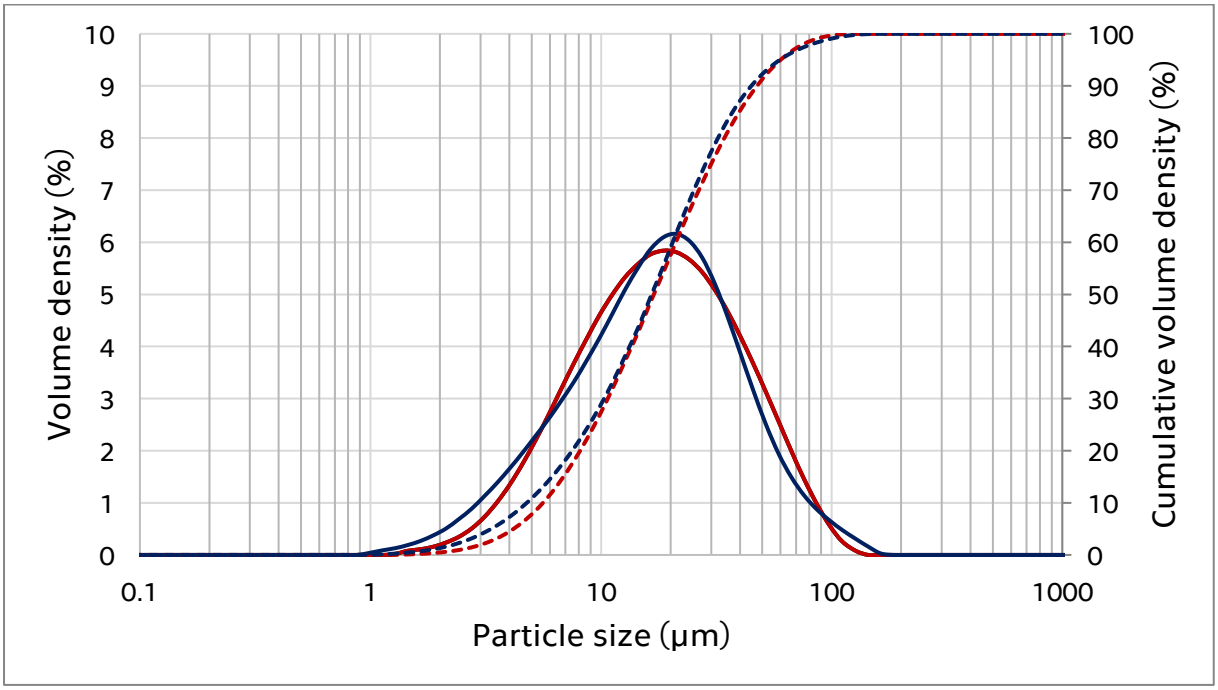

Fig. 11 – Volume distribution of the feedstock NiTi powder particle sizes.

As can be seen from the graphs and from Table 2, there is a large difference between the number distribution and the volume distribution. This is due to discrepancy in size of the large titanium particles and the much smaller nickel particles. While the thin Ni particles are numerous, their cumulative volume is very small compared to the bigger Ti particles. For the feeding principles in all

thermal spray methods, including cold spray, the volume distribution is the more important characteristic of the two. This said, the D_{10}–D_{90} range of cca 6–54 µm is suitable for the CS method.

The effect of the ultrasonic vibrations on each distribution is also different. The number distribution shifted more towards smaller particles sizes, while the effect on the volume distribution was less pronounced. In line with the SEM observation, this suggests that the smaller chain-like nickel particles are loosely bonded and tend to break up, while the large titanium particles are solid and can withstand certain mechanical loading.

Table 2 – Selected percentiles of the particle size distribution.

Measured density	Ultrasound	Percentiles		
		D_{10} (µm)	D_{50} (µm)	D_{90} (µm)
Number	No	1.69	3.2	7.73
Number	Yes	1.14	2.03	5.17
Volume	No	6.34	19.3	54
Volume	Yes	5.4	18.8	51

4.2 Coating

Despite the lack of previous spray parameters optimization, the produced coatings are very compact. The only – very scarce – porosity detected was concentrated in the uppermost layer that did not undergo the hammering effect from subsequent torch passes (see Fig. 12). The thickness of the coating is about 300 µm. The surface of the coating is rather rough and irregular; thus the thickness varies by several micrometers.

The coating is not homogeneous, but rather consists of particles of two different compositions. This is a consequence of the used powder not being an alloy, but rather a blend of Ni and Ti. In the coating, the individual particles correspond to either pure Ni, or pure Ti, easily distinguishable in the SEM micrographs (nickel, being the heavier element, appears brighter, while titanium appears darker). This conclusion is also supported by the EDX elemental mapping (see Fig. 13).

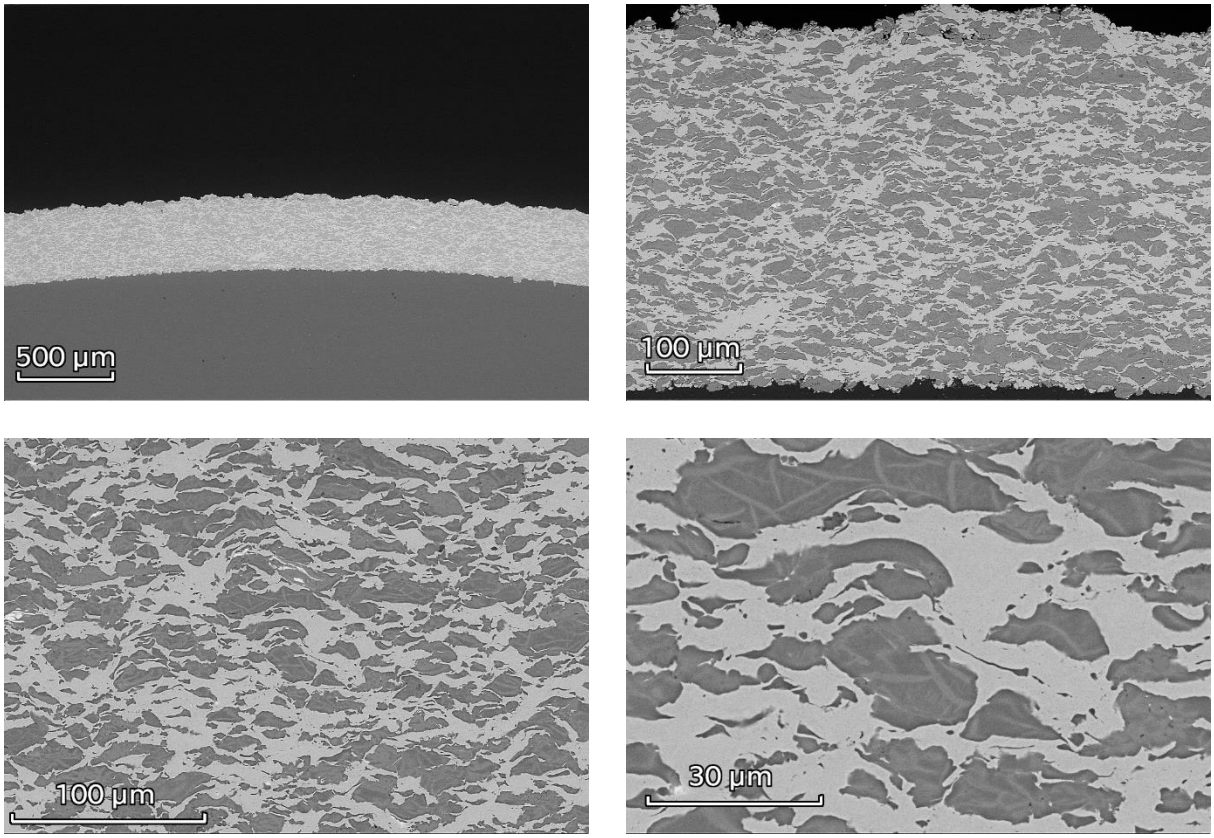

Fig. 12 – Microstructure of the cold sprayed NiTi coating at various magnifications.

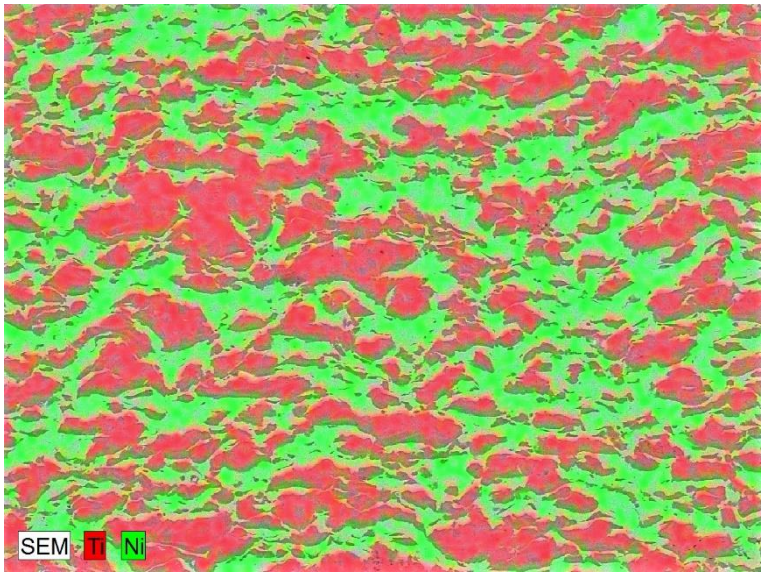

Fig. 13 – Elemental mapping of the cold sprayed NiTi coating.

Comparison of the composition of the powder as determined by quantitative EDX measurements with the coating measurements shown in Table 3 shows that the cold spraying process exhibits slightly preferential deposition of nickel. As the particle morphology should trigger a preferential deposition of titanium over nickel, this result means that the deformability of the two elements has prevailed

over the particle morphology: nickel has a more deformable FCC crystal lattice whereas α-titanium has a less deformable HCP lattice [6]. Still, the difference is only marginal and shows the suitability of the CS process for such dissimilar materials deposition.

This is supported by the results of XRD analysis (the measured spectrum is shown in Fig. 14). A slight increase in the amount of nickel was also measured here, caused by its preferential deposition over Ti. In a similar manner, the decrease of amount of titanium hydride can be considered a consequence of the same phenomenon. This is due to its brittleness and low plasticity, leading to lower deposition efficiency [21].

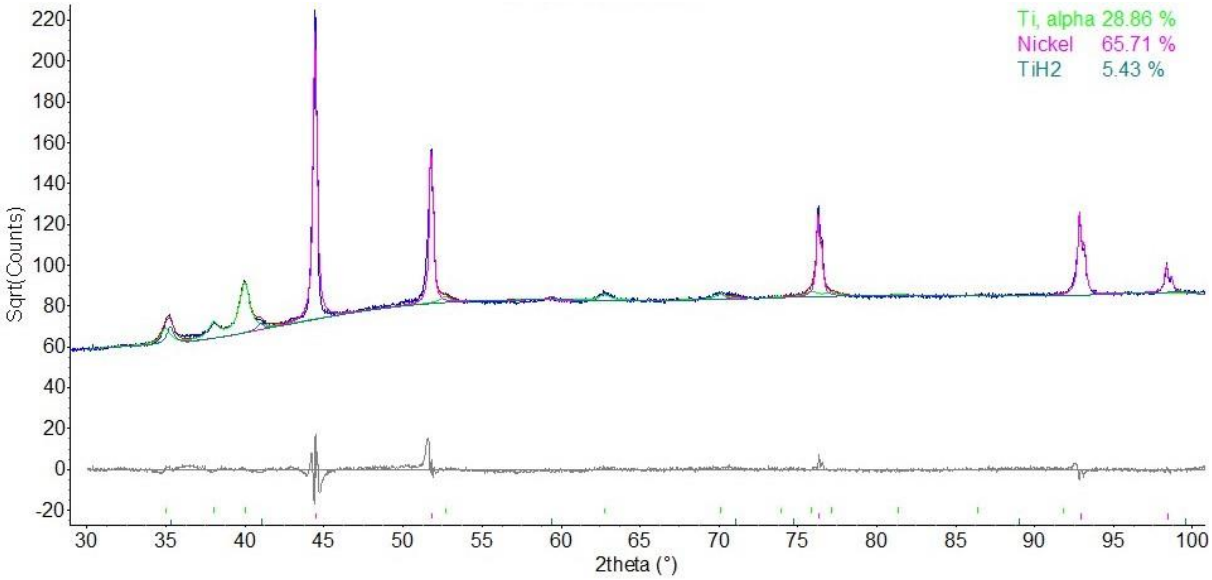

Fig. 14 – XRD diffraction spectrum of the coating.

Similar to the powder results, the results of the XRD analysis of the coating are also rather different from those of the EDX measurements, their comparison is shown in Table 3.

Table 3 - Comparison of the coating composition data.

Source	Ti wt%	Ni wt%	TiH_2 wt%
EDX powder	54.1	45.9	-
EDX coating	52.4	47.6	-
XRD powder	28.3	63.5	8.2
XRD coating	28.9	65.7	5.4

5 Conclusions

This thesis focused on the analysis of a NiTi alloy powder and the respective coating using cold spray. The morphology of the powder and the coating was examined using SEM, chemical composition was assessed using EDX, phase composition was assessed using XRD and particle size distribution of the powder was determined using laser diffraction. The following conclusion can be drawn from the results of the analyses:

- The powder contains highly irregular particles, comprising of two distinct morphologies: larger oval-shaped titanium particles and smaller, elongated thin nickel particles.
- Most particles fall within the size range of 1–8 µm, but these are rarely deposited in CS. Majority of the total volume is constituted by particles of sizes 6–54 µm that are suitable for the CS process.
- The chemical composition of the powder does not correspond to that stated by the manufacturer, with a higher titanium content. Further, the powder is a mechanical blend of the two elements, rather than their alloy.
- Aside from pure Ni and Ti, the powder also contains titanium hydride, probably a consequence of the Ti production process.
- Consequently, the respective coating is not homogeneous, but consists of particles of two distinct phases instead.
- The composition of the coating as compared to the powder has changed due to a preferential deposition during cold spray. This was influenced more by the deformability of the two components of the powder than by their morphology.
- The phase composition determined by XRD does not agree with the EDX results. The reason for this discrepancy is currently under investigation.

Figures list

Tables list

References

[1] PAPYRIN, Anatolii, Vladimir KOSAREV, Sergey KLINKOV, Anatolii ALKIMOV a Vasily FOMIN. *Cold Spray Technology*. 1st Edition. Amsterdam: Elsevier, 2006. ISBN 978-008-0451-558.

[2] SCHMIDT, Tobias, Hamid ASSASI a Frank GÄRTNER. From Particle Acceleration to Impact and Bonding in Cold Spraying. *Journal of Thermal Spray Technology*. 2009, **18**(5-6), 794-808. Dostupné z: doi:https://doi.org/10.1007/s11666-009-9357-7

[3] MORIDI, Atieh, Mostafa HASSANI-GANGARAJ, Mario GUAGLIANO a Ming DAO. Cold spray coating: review of material systems and future perspectives. *Surface Engineering*. 2014, **30**(6), 369-395. Dostupné z: doi:https://doi.org/10.1179/1743294414Y.0000000270

[4] ASSADI, Hamid, Heinrich KREYE, Frank GÄRTNER a Thomas KLASSEN. Cold spraying – A materials perspective. *Acta Materialia*. 2016, (116), 382-407. Dostupné z: doi:https://doi.org/10.1016/j.actamat.2016.06.034

[5] RAOELISON, Rija, Christophe VERDY a Hanlin LIAO. Cold gas dynamic spray additive manufacturing today: Deposit possibilities, technological solutions and viable applications. *Materials & Design*. 2017, (133), 266-287. Dostupné z: doi:https://doi.org/10.1016/j.matdes.2017.07.067

[6] HLUCHÝ, Miroslav, Rudolf PAŇÁK a Oldřich MODRÁČEK. *Strojírenská technologie 1: 2. díl. Metalografie a tepelné zpracování*. 3. přeprac. vyd. Praha: Scientia, 2002. ISBN 80-718-3265-0.

[7] Cold Spray Additive Manufactured Rocket nozzle. In: *Impact Innovations* [online]. 2020 [cit. 2022-11-15]. Dostupné z: https://impact-innovations.com/en/applications/rocket-nozzle/

[8] CHAMPAGNE, Victor K., ed. *The Cold Spray Materials Deposition Process: Fundamentals and Applications*. 1st Edition. Woodhead Publishing, 2007. ISBN 978-1-84569-181-3.

[9] HASSANI-GANGARAJ, Mostafa, David VEYSSET, Keith NELSON a Christopher SCHUH. Supersonic Impact of Metallic Micro-particles. *ArXiv*. 2016. Dostupné z: doi:https://doi.org/10.48550/arXiv.1612.08081

[10] GRUJICIC, Mica, C. ZHAO, William DEROSSET a Dennis HELFRITCH. Adiabatic shear instability based mechanism for particles/substrate bonding in the cold-gas dynamic-spray process. *Materials & Design*. 2004, (25), 681-688. Dostupné z: doi:https://doi.org/10.1016/j.matdes.2004.03.008

[11] HUSSAIN, T., D. MCCARTNEY, P. SHIPWAY a D. ZHANG. Bonding mechanism in Cold Spraying: The contributions of Metallurgical and Mechanical Components. *Journal of Thermal Spray Technology*. 2009, **18**(3), 364–379. Dostupné z: doi:https://doi.org/10.1007/s11666-009-9298-1

[12] YIN, Shuo, Jan CIZEK, Jan CUPERA et al. Formation conditions of vortex-like intermixing interfaces in cold spray. *Materials & Design*. 2021, **200**, 1-10. ISSN 02641275. Dostupné z: doi:10.1016/j.matdes.2020.109444

[13] OTSUKA, Kazuhiro a C. WAYMAN, ed. *Shape Memory Materials*. 1st Edition. Cambridge University Press, 1999. ISBN 9780521663847.

[14] JANI, Jaronie, Martin LEARY a Aleksandar SUBIC. A review of shape memory alloy research, applications and opportunities. *Materials & Design (1980-2015)*. 2014, (56), 1078-1113. Dostupné z: doi:https://doi.org/10.1016/j.matdes.2013.11.084

[15] BUEHLER, William, J. GILFRICH a R. WILEY. Effect of Low-Temperature Phase Changes on the Mechanical Properties of Alloys near Composition TiNi. *Journal of Applied Physics*. 1963, **34**, 1475–1477. Dostupné z: doi:https://doi.org/10.1063/1.1729603

[16] LOBO, Paulo, João ALMEIDA a Luís GUERREIRO. Shape Memory Alloys Behaviour: A Review. *Procedia Engineering*. 2015, (114), 776-783. Dostupné z: doi:https://doi.org/10.1016/j.proeng.2015.08.025

[17] ATTEBERRY, Jonathan. How Scanning Electron Microscopes Work. In: *How Stuff Works* [online]. Marina del Rey: HowStuffWorks, 2009 [cit. 2023-03-22]. Dostupné z: https://science.howstuffworks.com/scanning-electron-microscope2.htm

[18] NANAKOUDIS, Antonis. EDX Analysis with SEM: How Does it Work?. In: *ThermoFisher Scientific* [online]. Waltham: Thermo Fisher Scientific, 2006 [cit. 2023-03-22]. Dostupné z: https://www.thermofisher.com/blog/materials/edx-analysis-with-sem-how-does-it-work/

[19] BRAGG, William a William BRAGG. The reflection of X-rays by crystals. *Proceedings of the Royal Society of London. Series A.* London: The Royal Society, 1913, **88**(605), 428-438. ISSN 0950-1207. Dostupné z: doi:http://doi.org/10.1098/rspa.1913.0040

[20] Laser Diffraction (LD). In: *Malvern Panalytical* [online]. Malvern: Malvern Panalytical Ltd, 2023 [cit. 2023-03-22]. Dostupné z: https://www.malvernpanalytical.com/en/products/technology/light-scattering/laser-diffraction

[21] SETOYAMA, Daigo, Junji MATSUNAGA, Hiroaki MUTA, Masayohi UNO a Shinsuke YAMANAKA. Mechanical properties of titanium hydride. *Journal of Alloys and Compounds*. 2004, **381**(1-2), 215-220. Dostupné z: doi:https://doi.org/10.1016/j.jallcom.2004.04.073